



Accuracy of classical force fields for polyethylene structures away from equilibrium

Keara G. Frawley¹, **Lihua Chen**, **Huan Tran**, **Naresh N. Thadhani**, **Rampi Ramprasad**¹, School of Materials Science and Engineering, Georgia Institute of Technology, 771 Ferst Drive NW, Atlanta, GA 30332, USA

Address all correspondence to Rampi Ramprasad at Rampi.Ramprasad@mse.gatech.edu

(Received 8 June 2023; accepted 20 November 2023)

Abstract

This study compares the performance of four classical force fields (FFs)—OPLS, PCFF, TraPPE-UA, and ReaxFF—with density functional theory (DFT) for modeling polyethylene (PE) configurations under extreme conditions. We evaluate their accuracy in predicting energies, forces, and stresses. Additionally, the FFs are used to generate a pressure–temperature phase diagram to compare PE's melting behavior against experimental observations. The results indicate that PCFF and OPLS exhibit the closest agreement with DFT, while PCFF, TraPPE-UA, and ReaxFF perform equally when compared to experimental data. This research provides valuable insights for complex simulations, such as high-pressure shock compression studies on PE.

Introduction

Polyethylene (PE), the most commonly used plastic, has a simple molecular structure with a repeat unit of $(C_2H_4)_n$, making it an ideal and significant polymer for computational studies. PE is commercially classified based on density, molecular weight, and processing conditions that impact its microstructural phases. In its manufactured form, PE is typically semicrystalline, containing both crystalline and amorphous regions.^[1] The equilibrium crystalline phase of PE is orthorhombic; however, when subjected to external stress, it undergoes a martensitic phase transformation, transitioning into the metastable monoclinic phase. This phase transition has been extensively documented as early as 1957.^[2–4] Consequently, when conducting computational studies on PE, it is crucial to employ methods capable of accurately capturing the behavior of all three phases.

Density Functional Theory (DFT)^[5,6] and classical force field (FF) based molecular dynamics (MD) simulations^[7] are two widely utilized tools for modeling material behavior. DFT calculations are considered highly accurate but computationally expensive. On the other hand, classical FF simulations are more computationally efficient, enabling the study of larger and more intricate systems. This is because classical FFs circumvent the rigorous quantum mechanical calculations needed for DFT by being parameterized based on experimental or DFT data. Numerous studies have validated classical FFs against DFT results, investigating various material systems such as ice,^[8] MOFs,^[9] and polymers,^[10] however a comprehensive comparison of these methods specifically for PE with a focus on its non-equilibrium phases has not yet been conducted.

This study aims to assess the ability of four classical FFs to reproduce the outcomes of DFT calculations concerning various phases of PE. The four FFs under consideration are

Optimized Potentials for Liquid Simulations (OPLS),^[11,12] the Polymer Consistent Force Field (PCFF),^[13] Transferable Potentials for Phase Equilibria United Atom (TraPPE-UA),^[14] and the Reactive Force Field (ReaxFF).^[15,16]

OPLS and PCFF are two of the most commonly used FFs for MD simulations involving polymers. They are both trained on experimental data, utilize well-established parameterized functional forms to accurately represent atomic interactions, and have a relatively low computational cost. TraPPE-UA is a united atom FF, where groups of C atoms are treated as a single pseudo-atom.^[17] This approach significantly reduces the computational cost by decreasing the number of individual atoms that need to be explicitly considered. TraPPE-UA is trained on a combination of experimental data and electronic structure calculations. Similar to OPLS, it employs Coulomb and Lennard–Jones potentials in a 12–6 form to parameterize non-bonded interactions.^[14]

The three aforementioned FFs (OPLS, PCFF, and TraPPE-UA) are classified as nonreactive FFs, meaning that the chemical bonds defined at the beginning of the simulation remain fixed throughout the simulation. In contrast, ReaxFF is a reactive FF capable of handling bond breakage and formation during the simulation, making it suitable for modeling chemical reactions. The parameters of ReaxFF are typically derived from first-principles calculations, such as DFT.^[15,16,18] Consequently, ReaxFF has higher computational costs compared to the other FFs examined in this study.

This study also aims to assess the predictive capability of the four FFs in determining the melting point of bulk PE. The melting point of a material corresponds to the temperature at which it transitions from a solid to a liquid state, typically accompanied by a significant decrease in density, such as in the case of PE. Previous investigations comparing experimental

and FF-calculated melting points have been conducted for poly(vinylidene fluoride) (PVDF)^[19] and perfluorinated alkanes.^[20] These studies measured the density of the materials over increasing temperatures and found that the FF predictions overestimate the melting temperature as compared to experimental values. Several factors could account for this outcome. First, the movement of very long polymer chains is constrained by periodic boundary conditions, making it more challenging for the simulated material to undergo melting. Second, surface and interface effects that exert significant control over the melting process may not be fully captured by the simulations.

The primary objective of this study is to determine whether classical FFs produce results comparable to DFT calculations and experiments for PE spanning diverse and extreme configurations. To achieve this, several steps are undertaken. First, *ab-initio* MD simulations are conducted to generate orthorhombic, monoclinic, and amorphous structures of PE. These simulations start from their respective equilibrium configurations and are run at room temperature, generating numerous configurations for each phase. The DFT energies, forces, and stresses of these configurations are obtained from the *ab-initio* MD run. Subsequently, the classical FF energies, forces, and stresses are calculated by applying the FF parameters and performing a static, classical MD calculation on the same configurations. A comparison is then made between the classical FF results and the “ground truth” DFT results obtained. In addition to the comparative analysis, a pressure–temperature phase diagram is constructed using classical MD simulations with each FF. These simulations are carried out over a range of pressures and temperatures to determine the melting point of the orthorhombic PE equilibrium configuration. The obtained melting behavior of the orthorhombic phase is then compared to experimental results. These calculations serve as a foundational reference for future, more complex simulations, such as classical MD runs involving high-pressure shock compression studies on PE. Such simulations are expected to generate atomic configurations significantly deviating from equilibrium.

Methods

Structure generation, DFT and classical FF calculations

To initiate the study, orthorhombic and monoclinic unit cells were constructed for PE using their crystalline lattice parameters (space groups Pnam and C2/m, respectively). Each unit cell contains 4 C groups. These structures were then expanded to a $1 \times 2 \times 5$ supercell size, resulting in a total of 120 atoms per structure. These configurations served as the initial structures for the respective phases.

For the generation of the initial amorphous structure, the orthorhombic supercell was used as a starting point. A classical MD simulation was performed using OPLS with Large-scale Atomic/Molecular Massively Parallel Simulator (LAMMPS).^[21] The MD run consisted of three stages: an NVT-MD run (constant Number of particles, Volume, and

Temperature) at 600 K for 1 ns, followed by an NPT-MD run (constant Number of particles, Pressure, and Temperature) at 600 K for 1 ns, and finally, another NPT-MD run at 300 K for 5 ns. The resulting density of the structure was verified to be close to experimental values ($\sim 0.85 \text{ g/cm}^3$) and was adopted as the initial amorphous structure.

Using the initial structures for each phase, DFT-based (*ab-initio*) NPT-MD simulations were carried out at 300 K for a total of 100 fs. The structure at each of the 200 timesteps were recorded for each phase. The DFT energy values, three force components, and six stress components were obtained for each configuration during this *ab-initio* MD run. Vienna Ab initio Simulation Package (VASP)^[22,23] was employed for all the *ab-initio* MD simulations. The calculations utilized the Perdew–Burke–Ernzerhof (PBE) functional,^[24] Projector Augmented Wave (PAW) potentials, and plane-wave basis functions with a kinetic energy cutoff of 400 eV^[25] and used $4 \times 2 \times 1$ k-point meshes. The vdW-DF functional was employed for van der Waals calculations.^[26]

Classical FF results were obtained using LAMMPS with all four FFs: OPLS, PCFF, TraPPE-UA, and ReaxFF. The 200 structures of each phase were subjected to static calculations. This process yielded classical FF energy values, three force components, and six stress components per structure. Since the LAMMPS calculations are static, the structures obtained are directly comparable to those used in the DFT calculations, and the only difference lies in the parameterization employed within the FFs.

In order to test how the force fields perform under non-zero pressure conditions, a similar procedure as mentioned above was performed. First, NPT-MD simulations were carried out at 300 K and 0.6 GPa for a total of 100 fs. Then, five structures from each phase were selected to examine. In this step, the energy, forces, and stresses of each high pressure structure was calculated using DFT and compared with results from the four force fields examined.

Phase diagram

To construct the pressure–temperature (P–T) phase diagram of orthorhombic PE, the melting point of the structure (representing the transition from the solid to the liquid phase) was calculated at various pressures. The methodology employed is based on the approach outlined in Chen.^[27] Each of the four FFs was applied to a $4 \times 2 \times 15$ supercell of orthorhombic PE (containing 720 atoms), the model size for which a convergence of the phase diagram is reached. NPT-MD simulations were performed for a duration of 0.5 ns, maintaining a pressure of 1 atm while varying the temperature within the range of 300–700 K. Throughout the simulation, the density of the system was recorded, and the final density value was determined by averaging the values over the last 100 ps of the run. A significant decrease in density with increasing temperature was indicative of the occurrence of melting. This process was repeated for additional pressures of 250, 500, 750, and

1000 atm. The melting temperature from each pressure was used to generate a P–T phase diagram.

Results and discussion

Energy

The energies of the generated structures were computed at P=0 and P=0.6 GPa using both DFT and the selected classical FFs and were compared using parity plots shown in

Fig. 1. To facilitate a comprehensive comparison, the energy values were adjusted relative to the perfect orthogonal crystal structure. The ideal scenario is for the FF results to align perfectly with the DFT results, represented by the dashed parity line with a root mean square error (RMSE) value of 0, indicating perfect replication. The RMSE and the determination coefficient R^2 values for all of the calculations are shown in Tables I and II, respectively. Based on the RMSE values, the performance of the FFs can be ranked from best

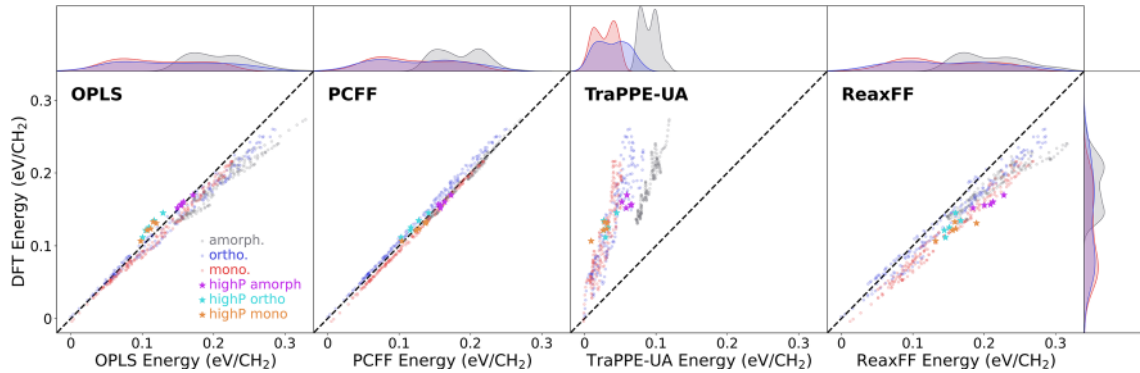


Figure 1. Comparison of DFT energy and OPLS, PCFF, TraPPE-UA, and ReaxFF (from left to right) energy. The energy is given for each of the crystal structure configurations at P=0 GPa (i.e., amorph. for amorphous, ortho. for orthorhombic, and mono. for monoclinic) and P=0.6 GPa (i.e., highP ortho and highP mono). The dashed line is a parity line, and above and to the right are distribution plots, showing the frequencies of each energy that occurs, which is difficult to tell from just the parity plots.

Table I. RMSE values for the energy, force, and stress calculations.

	phase	OPLS			PCFF			ReaxFF			TraPPE-UA		
Energy (eV/CH ₂)	amorph	0.027			0.004			0.035			0.096		
		(0.002)			(0.003)			(0.048)			(0.099)		
	mono	0.011			0.006			0.032			0.096		
		(0.013)			(0.004)			(0.038)			(0.098)		
ortho	0.014			0.009			0.019			0.106			
		(0.016)			(0.007)			(0.027)			(0.096)		
Force (eV/Å-CH ₂)	amorph	X	Y	Z	X	Y	Z	X	Y	Z	X	Y	Z
		0.480	1.109	1.313	0.225	1.061	1.273	1.865	1.842	1.959	0.498	0.977	1.230
	(0.945)	(1.102)	(1.299)	(1.032)	(1.224)	(1.327)	(2.311)	(2.532)	(2.148)	(0.620)	(1.048)	(1.203)	
	mono	0.274	0.873	1.186	0.106	0.916	1.182	0.449	3.017	1.564	0.560	0.859	1.137
		(0.930)	(1.192)	(1.152)	(0.991)	(1.296)	(1.152)	(1.156)	(3.545)	(1.336)	(0.877)	(1.105)	(1.156)
	ortho	0.476	1.264	1.411	0.204	1.278	1.356	2.047	2.543	1.927	0.529	1.120	1.330
	(0.856)	(1.146)	(1.430)	(0.892)	(1.250)	(1.460)	(2.510)	(2.639)	(1.658)	(0.873)	(1.068)	(1.377)	
Stress (GPa)	NORMAL	XX	YY	ZZ	XX	YY	ZZ	XX	YY	ZZ	XX	YY	ZZ
		0.329	0.498	0.995	1.872	2.033	0.637	4.780	3.850	6.795	2.082	2.001	1.042
	(0.826)	(1.021)	(1.348)	(1.816)	(1.945)	(0.794)	(7.753)	(6.696)	(12.673)	(0.982)	(1.294)	(1.402)	
	amorph	1.551	0.816	1.251	2.870	1.451	1.169	0.614	10.824	12.006	2.925	1.907	0.444
		(1.775)	(0.798)	(1.944)	(3.045)	(1.356)	(1.869)	(1.479)	(13.944)	(16.024)	(1.724)	(1.547)	(1.380)
	mono	0.798	1.508	1.341	2.104	1.791	1.507	5.973	5.269	13.805	2.515	2.181	0.599
		(1.227)	(2.067)	(1.961)	(1.936)	(1.759)	(1.965)	(7.822)	(6.216)	(16.303)	(1.175)	(2.178)	(0.478)
	SHEAR	XY	XZ	YZ	XY	XZ	YZ	XY	XZ	YZ	XY	XZ	YZ
		0.231	0.531	0.588	0.107	0.616	0.605	0.381	0.916	0.694	0.404	0.545	0.576
	(0.293)	(0.336)	(0.243)	(0.192)	(0.281)	(0.199)	(0.505)	(0.564)	(0.361)	(0.778)	(0.531)	(0.531)	
	amorph	0.169	0.768	0.765	0.165	0.789	0.823	1.265	0.910	1.067	0.403	0.739	0.817
		(0.365)	(0.464)	(0.646)	(0.156)	(0.543)	(0.588)	(1.447)	(0.814)	(0.620)	(2.002)	(0.633)	(0.619)
mono	0.445	1.213	1.039	0.167	1.157	1.075	0.530	1.353	1.218	1.199	1.220	1.058	
	(0.217)	(0.167)	(0.482)	(0.077)	(0.098)	(0.168)	(0.392)	(0.297)	(0.223)	(0.725)	(0.367)	(1.143)	

The data in parentheses are for the high pressure calculations and are colored to match the figures.

Table II. R^2 values for the energy, force, and stress calculations.

	phase	OPLS			PCFF			ReaxFF			TraPPE-UA			
Energy	amorph	0.951			0.993			0.774			0.885			
		(0.988)			(0.845)			(0.896)			(0.050)			
	mono	0.995			0.999			0.985			0.827			
		(0.919)			(0.996)			(0.663)			(0.793)			
ortho	0.989			0.998			0.977			0.840				
		(0.969)			(0.991)			(0.616)			(0.468)			
Force	amorph	X	Y	Z	X	Y	Z	X	Y	Z	X	Y	Z	
		0.688	0.676	0.884	0.921	0.920	0.955	0.206	0.342	0.479	0.587	0.553	0.865	
	(0.078)	(0.073)	(0.090)	(0.075)	(0.045)	(0.101)	(0.035)	(0.022)	(0.037)	(0.503)	(0.634)	(0.901)		
	0.819	0.859	0.920	0.979	0.909	0.966	0.615	0.117	0.561	0.145	0.679	0.932		
	(0.029)	(0.003)	(0.007)	(0.026)	(0.006)	(0.010)	(0.013)	(0.012)	(0.024)	(0.023)	(0.059)	(0.031)		
	0.701	0.801	0.905	0.934	0.947	0.973	0.219	0.266	0.590	0.555	0.607	0.933		
		(0.177)	(0.296)	(0.163)	(0.195)	(0.281)	(0.178)	(0.073)	(0.048)	(0.099)	(0.121)	(0.236)	(0.177)	
Stress	NORMAL	amorph	XX	YY	ZZ	XX	YY	ZZ	XX	YY	ZZ	XX	YY	ZZ
		0.975	0.909	0.753	0.999	0.994	0.858	0.836	0.795	0.330	0.061	0.065	0.258	
	(0.958)	(0.852)	(0.964)	(0.995)	(0.904)	(0.982)	(0.119)	(0.160)	(0.684)	(0.339)	(0.165)	(0.941)		
	0.908	0.881	0.830	0.995	0.996	0.912	0.940	0.394	0.596	0.002	0.126	0.748		
	(0.958)	(0.673)	(0.713)	(0.992)	(0.965)	(0.723)	(0.941)	(0.709)	(0.286)	(0.704)	(0.046)	(0.469)		
	0.916	0.959	0.447	0.999	0.998	0.857	0.759	0.680	0.604	0.003	0.002	0.529		
	(0.939)	(0.979)	(0.241)	(0.995)	(0.967)	(0.568)	(0.794)	(0.787)	(0.055)	(0.592)	(0.108)	(0.379)		
	SHEAR	amorph	XY	XZ	YZ	XY	XZ	YZ	XY	XZ	YZ	XY	XZ	YZ
		0.758	0.203	0.235	0.959	0.162	0.211	0.569	0.138	0.088	0.066	0.026	0.236	
	(0.967)	(0.959)	(0.976)	(0.982)	(0.956)	(0.980)	(0.933)	(0.629)	(0.768)	(0.630)	(0.947)	(0.650)		
	0.905	0.070	0.018	0.960	0.056	0.034	0.151	0.001	0.019	0.108	0.160	0.007		
	(0.997)	(0.557)	(0.582)	(0.998)	(0.537)	(0.630)	(0.747)	(0.409)	(0.664)	(0.718)	(0.118)	(0.696)		
0.932	0.598	0.388	0.986	0.397	0.236	0.860	0.311	0.188	0.000	0.827	0.729			
	(0.989)	(0.922)	(0.974)	(0.996)	(0.965)	(0.990)	(0.965)	(0.781)	(0.959)	(0.951)	(0.664)	(0.090)		

The data in parentheses are for the high pressure calculations and are colored to match the figures.

to worst as follows: PCFF, OPLS, ReaxFF, and TraPPE-UA. The poor performance of TraPPE-UA can be attributed to its treatment of each C group as a pseudo-atom, resulting in lower accuracy compared to the other FFs. However, it is worth noting that all FFs exhibit RMSE values below or around 0.1 eV/C , indicating a generally strong agreement between the FF and DFT energy values. The R^2 values show similar trends, with PCFF having a value of almost 1 and TraPPE-UA having the lowest value. However, the R^2 values of the high pressure structures show that TraPPE-UA cannot capture the desired behavior, though the other three force fields can.

The distribution plots, located above and to the right of the parity plots, illustrate the energy distributions for each phase. These plots reveal that none of the methods is capable of distinguishing between the equilibrium (orthorhombic) and metastable (monoclinic) crystalline structures. Despite experimental evidence supporting the orthorhombic phase as the equilibrium structure, both DFT and the four FFs calculate the monoclinic phase to have lower energy. It is known, however, that the energy difference between the two phases is expected to be small,^[28] thus it is not unexpected that the methods cannot differentiate the equilibrium phases. Additionally, the RMSE values do not significantly differ among the three phases, indicating that all FFs demonstrate similar accuracy regardless of whether the structure is orthorhombic, monoclinic, or amorphous.

Force

Figure 2 displays the parity plots depicting the comparison between the forces calculated using DFT and those computed using the selected FFs. Unlike energy, which is a global quantity defined for the entire system, the force is experienced by an individual atom, defined as the negative of the first derivative of the energy with respect to the atomic position. Each atom has three force components (x, y, and z) associated with it. To ensure a fair comparison between the all-atom and united-atom approaches, the presented results represent the net forces acting on each C unit. This was achieved by grouping the individual atoms into the same C clusters employed by TraPPE-UA and summing the forces along the x, y, and z directions.

For the zero-pressure structures, as Fig. 2 demonstrates, PCFF exhibits excellent performance, closely followed by OPLS which only slightly deviates from the ideal parity line. Unlike the results for energy, TraPPE-UA performs better than ReaxFF. The force distribution of ReaxFF appears more dispersed, with a slope that deviates from the parity line, indicating lower accuracy when compared to the DFT results (as evidenced by the higher RMSE values). The reason TraPPE-UA appears to be better than ReaxFF may come from the united-atom model of TraPPE-UA. To be more specific, all the atomic forces between the “real” atoms, which are generally “not good” using empirical force fields, are ignored in the case of TraPPE-UA while they are explicitly computed and contributed

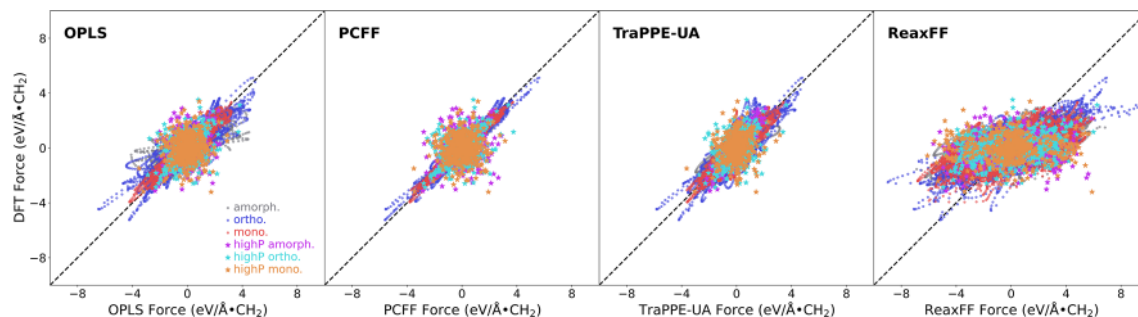


Figure 2. Comparison of DFT forces (x , y , and z) and OPLS, PCFF, TraPPE-UA, and ReaxFF (from left to right) force for each of the crystal structure configurations at $P=0$ GPa (i.e., amorph. for amorphous, ortho. for orthorhombic, and mono. for monoclinic) and $P=0.6$ GPa (i.e., highP ortho and highP mono). The dashed line is a parity line.

to the displayed results of ReaxFF. Therefore, when “not good” results are suppressed, TraPPE-UA artificially appears to be better than ReaxFF. The forces from the high-pressure structures, however, are not well-aligned with the DFT results. This indicates that the forcefields have a difficult time replicating the forces found in high pressure configurations.

Stress

The stress tensor has nine components, but it is often reduced to just six (each of three normal and shear components) due to symmetry restrictions. Therefore, the stress tensor becomes:

$$\begin{bmatrix} xx & xy & x \\ yx & yy & y \\ x & y & \end{bmatrix} \rightarrow \begin{bmatrix} xx & xy & x \\ & yy & y \\ & & \end{bmatrix}$$

Figure 3 presents parity plots depicting the agreement between the six stress components calculated using DFT and the corresponding values obtained from the FFs. In the top row, representing the normal stress components xx and yy , OPLS demonstrates the closest replication of the DFT behavior, with PCFF performing slightly less accurately. Although ReaxFF exhibits a larger spread of stresses, it still captures the trend of the DFT results. On the other hand, the xx , yy , x and y stress components computed using TraPPE-UA do not show correlations with DFT results, and thus TraPPE-UA is the least accurate among the FFs for these two components. Notably, the x and y components for the monoclinic phase can be distinguished from the orthorhombic phase with all of the FFs, except for OPLS. In these cases, the RMSE values for the orthorhombic phase are generally lower than those for the monoclinic phase.

The xy stress component (middle row), aligned along the polymer chain direction, is the most challenging to capture accurately, likely due to the larger and more flexible range of motion in that direction. The three shear stress components (x , x , y) shown in the bottom row are indistinguishable from each other and are combined in a single plot for each FF. Remarkably, the shear stress components exhibit better agreement with the DFT values compared to the other stress components. PCFF and OPLS show the closest correspondence to the DFT results

for the shear stress components, while TraPPE-UA and ReaxFF demonstrate comparatively poorer performance. These trends are also exhibited with the high pressure structure results.

Below are the data tables containing RMSE and R^2 values for the energy, force, and stress calculations.

Phase diagram

In Fig. 4, the P - T phase diagram is presented, constructed based on the method described in Chen.^[27] The density of orthorhombic PE is plotted at various pressures and temperatures for the four FFs, along with the experimental data^[29] and thermodynamic integration simulations data obtained from^[30] for comparison. The experimental values for density at temperatures above room temperature were not reported. Figure 4(a) shows the example of the density of PE at 1 atm from 300 to 700 K as calculated by the four FFs. From this graph, the melting temperature can be identified by the sharp decrease in density, indicated by the dashed vertical lines. These melting temperatures were determined for each of the four FF methods over a range of pressures (1, 250, 500, 750, 1000 atm) and plotted as a P - T phase diagram [Fig. 4(b)], where the experimental values are also displayed.

From the results, it can be observed that PCFF, TraPPE-UA, and ReaxFF are closest in temperature to the experimental values. PCFF and ReaxFF also capture the shape of the experimental curve more accurately. All of the FF methods, however, tend to overpredict the experimental values. There is about a 50–100 K error on these predictions compared to experimental and simulation data. Among the FFs, OPLS deviates the most from the experimental data. Overall, while the FF methods do not perfectly replicate the exact experimental melting temperatures, they are able to capture the general trend of melting. This discrepancy between FF predictions and experimental results is not unexpected, as previous studies on other systems, such as PVDF and perfluorinated alkanes, have also shown overestimation of melting temperatures by FF methods compared to experimental data. This discrepancy can be attributed to surface tension and interface effects that are more pronounced at the molecular scale but not fully captured in experiments. It can be concluded that

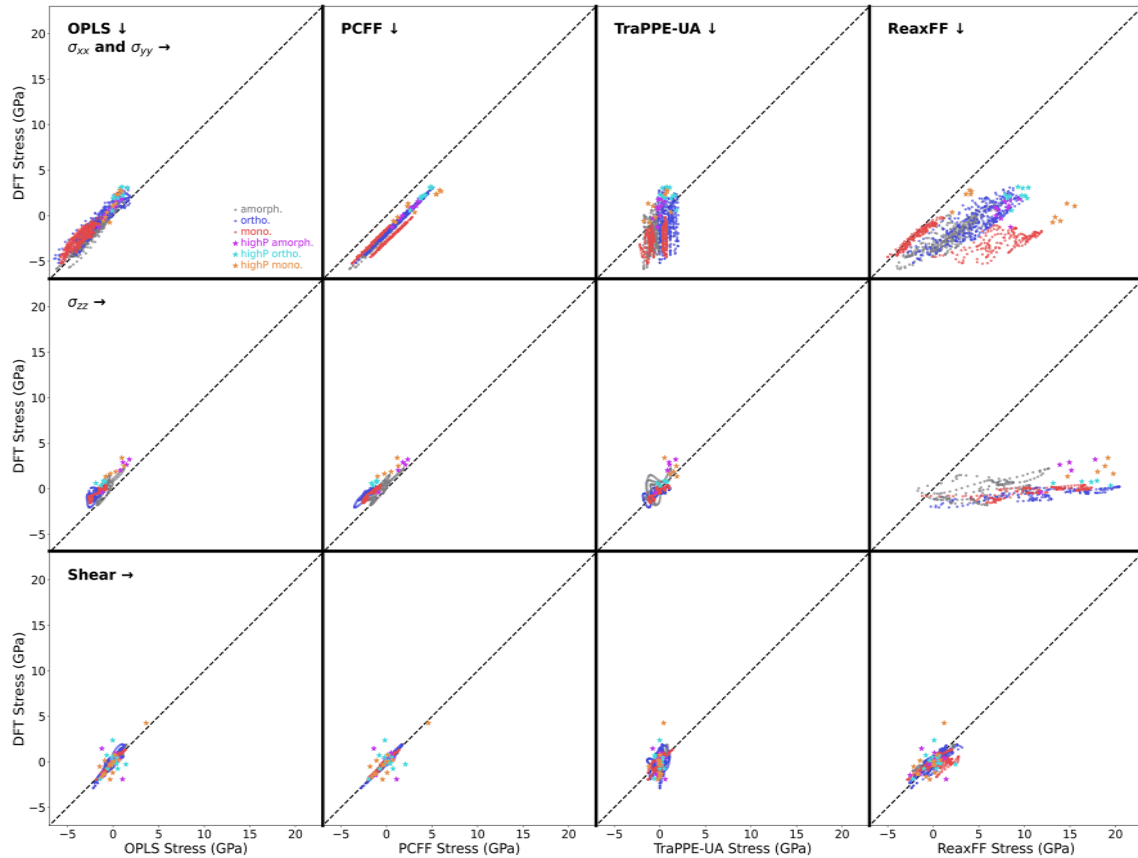


Figure 3. Comparison of DFT stress and OPLS, PCFF, TraPPE-UA, and ReaxFF (from left to right) stress for each of the crystal structure configurations at $P=0$ GPa (i.e., amorph. for amorphous, ortho. for orthorhombic, and mono. for monoclinic) and $P=0.6$ GPa (i.e., highP ortho and highP mono). Top: σ_{xx} and σ_{yy} , Middle: σ_{zz} , and Bottom: Shear. The dashed line is a parity line.

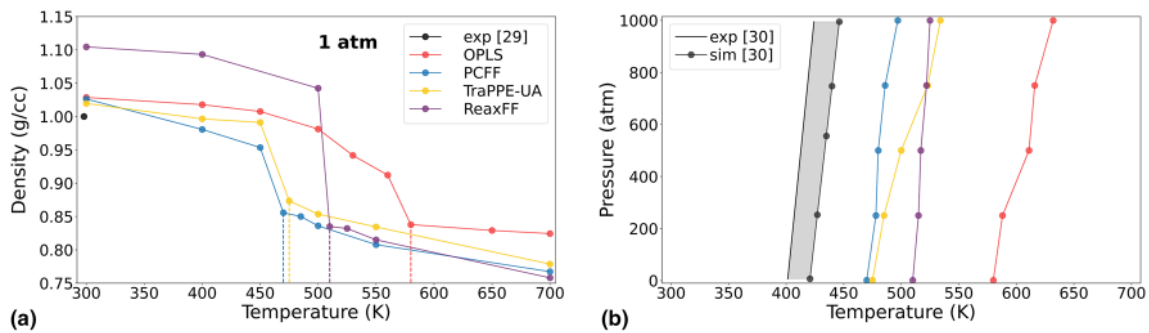


Figure 4. (a) Density evolution over temperature for 1 atm with the dashed lines indicating the melting temperature. (b) pressure–temperature phase diagram for all FFs. Experimental results from Ref. 29 are shown as a straight black line, while results from thermodynamic integration approach are given in black dots and the shaded area between them is the error difference between the methods.

PCFF, TraPPE-UA, and ReaxFF perform reasonably well under these circumstances, while OPLS falls short in replicating the experimental behavior.

Conclusions

In this study, we have conducted a comprehensive comparison of four different classical force fields (FFs) to assess their ability to replicate the behavior of non-equilibrium structures

of polyethylene (PE) using density functional theory (DFT) as a benchmark. The FFs are primarily parameterized based on equilibrium structures, and our goal was to investigate their performance in simulating structures away from equilibrium. Our analysis focused on energy, force, and stress calculations for the generated structures using each FF. The results indicate that the FFs can effectively replicate the energy values, with PCFF showing the best performance, closely followed by OPLS. This suggests that PCFF and OPLS can be trusted for accurate energy

calculations in simulations involving non-equilibrium structures of PE.

When it comes to force and stress calculations, the accuracy decreases, however PCFF and OPLS still demonstrate favorable performance compared to TraPPE-UA and ReaxFF. Among the four FFs, ReaxFF stands out as the only one capable of capturing bond breaking and chemical reactions. Although the overall performance of ReaxFF is not as strong as PCFF and OPLS, it outperforms TraPPE-UA and can be a suitable choice for simulations involving reactive processes in PE.

Based on the results, PCFF and OPLS emerge as the top choices for accurate simulations of non-equilibrium structures of PE. The capabilities of ReaxFF in handling chemical reactions and bond breaking make it a viable option for reactive simulations of PE. The findings of this study pave the way for future investigations involving non-equilibrium structures of PE, particularly in high-pressure shock-compression or high-strain-rate deformation scenarios. The promising performance of PCFF and ReaxFF will be instrumental in advancing simulations of such complex phenomena.

Acknowledgments

This work supported KGF by the Department of Defense (DoD) through the National Defense Science & Engineering Graduate (NDSEG) Fellowship Program.

Author contributions

The authors confirm contribution to the paper as follows: study conception and design: RR; calculations: KGF, LC, HT; analysis and interpretation of results: all; draft manuscript preparation: all.

Data availability

All data and code generated during this study is available by request.

Declarations

Conflict of interest

On behalf of all authors, the corresponding author states that there is no conflict of interest.

References

- D. Jeremic, Ullmann's Encyclopedia of Industrial Chemistry, (Wiley-VCH, Weinheim, 2014) https://doi.org/10.1002/14356007.a21_487.pub3
- P.W. Teare, D.R. Holmes, J. Polym. Sci. (1956). <https://doi.org/10.1002/pol.1957.1202410724>
- Y. Takahashi, T. Ishida, M. Furusaka, J. Polym. Sci. B: Polym. Phys. (1988). <https://doi.org/10.1002/polb.1988.090261107>
- K.E. Russell, B.K. Hunter, R.D. Heyding, Polymer (1997). [https://doi.org/10.1016/S0032-3861\(96\)00643-X](https://doi.org/10.1016/S0032-3861(96)00643-X)
- P. Hohenberg, W. Kohn, Phys. Rev. (1964). <https://doi.org/10.1103/PhysRev.136.B864>
- W. Kohn, L.J. Sham, Phys. Rev. (1965). <https://doi.org/10.1103/PhysRev.140.A1133>
- B.J. Alder, T.E. Wainwright, J. Chem. Phys. (1959). <https://doi.org/10.1063/1.1730376>
- C. Wang, Y. Xue, C. Wang, D. Han, Comput. Mater. Sci. (2020). <https://doi.org/10.1016/j.commatsci.2020.109546>
- J.A. Greathouse, M.D. Allendorf, J. Phys. Chem. C (2008). <https://doi.org/10.1021/jp076853w>
- T.R. Mattsson, J.M.D. Lane, K.R. Cochrane, M.P. Desjarlais, A.P. Thompson, F. Pierce, G.S. Grest, Phys. Rev. B (2010). <https://doi.org/10.1103/PhysRevB.81.054103>
- W.L. Jorgensen, J. Tirado-Rives, J. Am. Chem. Soc. (1988). <https://doi.org/10.1021/ja00214a001>
- E.K. Watkins, W.L. Jorgensen, J. Phys. Chem. A (2001). <https://doi.org/10.1021/jp004071w>
- H. Sun, S.J. Mumby, J.R. Maple, A.T. Hagler, J. Am. Chem. Soc. (1994). <https://doi.org/10.1021/ja00086a030>
- S.J. Keasler, S.M. Charan, C.D. Wick, I.G. Economou, J.I. Siepmann, J. Phys. Chem. (2012). <https://doi.org/10.1021/jp302975c>
- A.C.T. Duin, S. Dasgupta, F. Lorant, W.A. Goddard, J. Phys. Chem. (2001). <https://doi.org/10.1021/jp004368u>
- T.P. Senftle, S. Hong, M.M. Islam, S.B. Kylasa, Y. Zheng, Y.K. Shin, C. Junkermeier, R. Engel-Herbert, M.J. Janik, H.M. Aktulga, T. Verstraelen, A. Grama, A.C.T. Duin, npj Comput. Mater. (2016). <https://doi.org/10.1038/npjcompumats.2015.11>
- C.D. Wick, M.G. Martin, J.I. Siepmann, J. Phys. Chem. (2000). <https://doi.org/10.1021/jp001044x>
- G. Shchygol, A. Yakovlev, T. Trnka, A.C.T. Duin, T. Verstraelen, J. Chem. Theory Comput. (2019). <https://doi.org/10.1021/acs.jctc.9b00769>
- E. Erdtman, K.C. Satyanarayana, K. Bolton, Polymer (2012). <https://doi.org/10.1016/j.polymer.2012.04.045>
- M. Tsigie, G.S. Grest, J. Phys. Chem. C (2008). <https://doi.org/10.1021/jp710678w>
- A.P. Thompson, H.M. Aktulga, R. Berger, D.S. Bolintineanu, W.M. Brown, P.S. Crozier, P.J. in't Veld, A. Kohlmeyer, S.G. Moore, T.D. Nguyen, R. Shan, Comput. Phys. Commun. (2022). <https://doi.org/10.1016/j.cpc.2021.108171>
- G. Kresse, J. Furthmüller, Phys. Rev. B (1996). <https://doi.org/10.1103/PhysRevB.54.11169>
- G. Kresse, D. Joubert, Phys. Rev. B (1999). <https://doi.org/10.1103/PhysRevB.59.1758>
- J.P. Perdew, K. Burke, Y. Wang, Phys. Rev. B (1996). <https://doi.org/10.1103/PhysRevB.54.16533>
- P.E. Blöchl, Phys. Rev. B (1994). <https://doi.org/10.1103/PhysRevB.50.17953>
- M. Dion, H. Rydberg, E. Schröder, D.C. Langreth, B.I. Lundqvist, Phys. Rev. Lett. (2005). <https://doi.org/10.1103/PhysRevLett.92.246401>
- L. Chen, Electronic Structure and Vibrational Behavior of Polyethylene: Role of Chemical, Morphological and Interfacial Complexity, Dissertation, University of Connecticut, 2017
- T. Yemni, R.L. McCullough, J Polym Sci B: Polym. Phys. (1973). <https://doi.org/10.1002/pol.1973.180110713>
- R. Androsch, M.L.D. Lorenzo, C. Schick, B. Wunderlich, Polymer (2010). <https://doi.org/10.1016/j.polymer.2010.07.033>
- C. Das, D. Frenkel, J. Chem. Phys. (2003). <https://doi.org/10.1063/1.1568934>

Publisher's Note Springer Nature remains neutral with regard to jurisdictional claims in published maps and institutional affiliations.

Springer Nature or its licensor (e.g. a society or other partner) holds exclusive rights to this article under a publishing agreement with the author(s) or other rightsholder(s); author self-archiving of the accepted manuscript version of this article is solely governed by the terms of such publishing agreement and applicable law.